USING MULTIPLE TENSOR DEFLECTION TO RECONSTRUCT WHITE MATTER FIBER TRACES WITH BRANCHING

Weihong Guo, Qingguo Zeng, Yunmei Chen

University of Florida, Dept. of Mathematics

Yijun Liu

University of Florida, Dept. of Psychiatry

ABSTRACT

The relationship between brain structure and complex behavior is governed by large-scale neurocognitive networks. Diffusion weighted imaging(DWI) is a noninvasive technique that can visualize the neuronal projections connecting the functional centers and thus provides new keys to the understanding of brain function. In this paper, we assume there are up to two diffusion channels at each voxel. A variational framework for 3D simultaneous smoothing and reconstruction of a multi-diffusion tensor field as well as a novel multi-tensor deflection(MTEND) algorithm for extracting white matter fiber traces based on the multi-diffusion tensor field are provided. By applying the proposed model to both synthetic data and human brain high angular resolution diffusion(HARD) magnetic resonance imaging(MRI) data of several subjects, we show the effectiveness of the model in recovering branching fiber traces. Superiority of the proposed model over existing models are also demonstrated.

1. INTRODUCTION

The assessment of connectivity and the reconstruction of 3D curves representing fiber traces are useful for both basic neuroanatomical research and disease detection. Diffusion imaging is based on magnetic resonance imaging technique which was introduced in mid 1980s [1]and provides a very sensitive probe for detecting biological tissue structure. The diffusion of water molecules in tissues over a time interval t on the displacement $\mathbf{r}$ can be described by a probability density function $p_t(\mathbf{r})$. p_t is related to diffusion weighted signal via a Fourier Transformation (FT) with respect to $\mathbf{q}$, which represents the diffusion sensitizing gradients, by

$$s(\mathbf{q}) = s_0 \int p_t(\mathbf{r}) e^{-i\mathbf{q}\cdot\mathbf{r}} d\mathbf{r}, \tag{1}$$

where s_0 is the signal in absence of gradients.

For Gaussian diffusion, p_t is assumed to be a Gaussian, (1) is then reduced to $s(\mathbf{q}) = s_0 e^{-b\mathbf{u}^T D\mathbf{u}}$, where D is a second order diffusion tensor, $b = t|\mathbf{q}|^2$ is the diffusion-weighting factor, and $\mathbf{u} = \mathbf{q}/|\mathbf{q}|$. Fractional anisotropy(FA) of D with eigenvalues $\lambda_1 \geq \lambda_2 \geq \lambda_3 > 0$ is defined as

$$FA = \sqrt{\frac{3}{2}} \sqrt{\frac{(\lambda_1 - \lambda_2)^2 + (\lambda_2 - \lambda_3)^2 + (\lambda_3 - \lambda_1)^2)}{(\lambda_1 + \lambda_2 + \lambda_3)^2}}. \tag{2}$$

However, it has been recognized that Gaussian model is inappropriate when there are different tissues with different tensors occupying the same voxel[2, 3, 4, 5]. A simple alternative is the partial volume model for two diffusion-tensor components. It assumes that p_t is a mixture of 2 Gaussians(in short, biGaussian). Then the diffusion is modelled by

$$s(\mathbf{q}) = s_0(f e^{-b\mathbf{u}^T D_1 \mathbf{u}} + (1-f) e^{-b\mathbf{u}^T D_2 \mathbf{u}}), \tag{3}$$

where $f \geq 0, 1-f \geq 0$ are considered as volume fractions of diffusion tensors D_1, D_2 respectively.

Considering the acquisition noise which corrupts data measurement,natural smoothness of $D_i(\mathbf{x}), i = 1, 2$ and $f(\mathbf{x})$ across voxels, we present a new variational method which simultaneously recovers and smoothes $D_i(\mathbf{x}), i = 1, 2$ and $f(\mathbf{x})$. We applied the biGaussian model to each voxel in the field while Parker et al [6] and Tuch et al. [7] applied it only to the voxels where the Gaussian model fits the data badly. Thus they required voxel classification which will incorporate error. Moreover, they did not consider denoising at all. Section 2 will explain in detail how to recover the smooth multi-diffusion tensor field.

Regarding reconstruction of white matter fiber traces, a widely used scheme is line propagation based on the principle eigenvector(PE) of the diffusion tensor[8, 9, 10].PE successfully determines the fiber direction in cases when there is a single fiber direction in each voxel. However, image noise will influence the direction of the major eigenvector. And as magnitude of anisotropy decreases, the uncertainty in the major eigenvector increases, at which tracking may be erroneous. Westin et.al [11] and Lazar et.al[12] used the entire tensor to deflect the estimated fiber trajectory. This algorithm is called tensor deflection(TEND). TEND is better than using PE in the sense that the previous one is less sensitive to image noise and is less erroneous in situation

of degenerated anisotropy. But it still has the problem of partial volume averaging of fiber direction.

In section 3, we will provide a new line propagation algorithm based on the smooth multi-tensor field. It keeps all the advantages of TEND and has two additional good properties: firstly, problem of partial volume averaging is automatically solved as it is based on multi-tensor field; secondly, it uses dynamically adjusted step size to keep total curvature of traces low, to appropriately terminate tracking and to increase algorithm accuracy.

2. RECONSTRUCTION OF MULTI-TENSOR FIELD IN HARD MRI

We assume the data acquisition noise is additive and the distribution $p_t(\mathbf{r})$ is a biGaussian. The goal of this section is to recover a smooth multi-tensor field $D_i(\mathbf{x}), i = 1, 2$ and $f(\mathbf{x})$ from the noisy HARD MRI data. To guarantee the positive definiteness of diffusion tensor D_1, D_2, by Cholesky factorization theorem, we let $D_i = L_i L_i^T$, for $i = 1, 2$, L_i is a lower triangular matrix with positive diagonal entries. Positiveness of the diagonal entries is enforced by setting them to be exponents of some other variables. Constraint $0 \leq f \leq 1$ is fulfilled through letting $f(\mathbf{x}) = .5 + \frac{\arctan(\omega(\mathbf{x}))}{\pi}$ which is an increasing smooth function of ω. For conciseness, we still use diagonal entries of L_1, L_2 and f themselves to set up the model. We use the following non-constrained minimization model:

$$\min_{L_1(\mathbf{x}), L_2(\mathbf{x}), f(\mathbf{x})} \int_\Omega (\sum_{i=1}^{2} \sum_{m=1}^{3} \sum_{n=1}^{m} \alpha |\nabla L_i^{mn}(\mathbf{x})| + \beta |\nabla f(\mathbf{x})|) d\mathbf{x}$$
$$+ \int_\Omega \int_0^{2\pi} \int_0^{\pi} |s_0(\mathbf{x})(f e^{-b\mathbf{u}^T L_1 L_1^T \mathbf{u}} + (1-f) e^{-b\mathbf{u}^T L_2 L_2^T \mathbf{u}})$$
$$- s(\mathbf{x}, \theta, \phi)|^2 sin\theta d\theta d\phi d\mathbf{x} \quad (4)$$

Where L_i^{mn} denotes the mn^{th} entry of L_i, α, β are used to control smoothness of L_i^{mn} and f and thus that of the tensor field. $\mathbf{u} = (sin\theta cos\phi, sin\theta sin\phi, cos\theta)^T$ with $0 \leq \theta < \pi$ and $0 \leq \phi < 2\pi$. The first two terms are the regularization terms, the last term is the nonlinear data fidelity term based on (3).

We employ a gradient descent scheme to solve the minimization problem(4). Initials of f, L_1, L_2 are carefully chosen to avoid sticking on local minima. How to select α, β is a challenging question. We use two criteria to control the choice: Firstly, it is well known that at locations with high FA values, single Gaussian diffusion is enough to describe the water molecule motion, thus f should be very close to 1 or 0 ; Secondly, images of ADC profile $\mathbf{u}^T D_i \mathbf{u}$ also help to evaluate smoothness of L_i^{mn}.

3. WHITE MATTER FIBER TRACTOGRAPHY

Results of (4) provide a smooth multi-tensor vector field and a smooth volume fraction field f, fiber tractography based on which is almost not sensitive to noise and thus more accurate. In this section, we will provide an improved line propagation algorithm for reconstructing white matter fiber traces. Line propagation scheme is defined by: $\mathbf{x}(t+1) = \mathbf{x}(t) + \mathbf{v}(t+1)\delta$, where $\mathbf{x}(t)$ is the position vector in R^3 of the streamline at time t, $\mathbf{v}(t+1)$ is a unit vector from the position $\mathbf{x}(t)$ to the next step $\mathbf{x}(t+1)$, and δ is the step size.

Based on DTI model, the widely used $\mathbf{v}(t+1)$ is the PE of the tensor at $\mathbf{x}(t)$. Due to the sensitivity of PE to noise and the ambiguity of PE at voxels with low anisotropy, Westin et.al [11] used the whole tensor D at $\mathbf{x}(t)$ to deflect $\mathbf{v}(t)$ to obtain $\mathbf{v}(t+1)$ as $D \cdot \mathbf{v}(t)$. This scheme is named as TEND. The multi-tensor deflection(MTEND) we will introduce is based on partial volume model (3), at each voxel, there are up to 2 diffusion tensors $D_i, i = 1, 2$, define

$$\mathbf{v}_i(t+1) = (1-\gamma)\mathbf{v}(t) + \gamma D_i \cdot \mathbf{v}(t) \quad (5)$$

Where $\gamma \in [0, 1]$ is a weight balancing previous fiber direction $\mathbf{v}(t)$ and the deflected fiber direction $D_i \cdot \mathbf{v}(t)$ which is normalized before being used. Normalization is essentially necessary as for human brain diffusion weighted MRI data, norm of $D_i \cdot \mathbf{v}(t)$ is usually in the order of 10^{-3}, tensor deflection without normalization would not contribute as much as expected.

To make following explanation concise, let $f_1 = f$ and $f_2 = 1 - f$. For $i = 1, 2$ we define step size corresponding to tensor D_i as $\delta_i = c f_i FA_i \mathbf{v}(t) \cdot \mathbf{v}_i(t+1)$ with c a fixed constant, FA_i the fractional anisotropy(FA) corresponding to tensor D_i. As we know, if f_i is very close to 0, channel D_i could be ignored; if FA_i is very low, anisotropy of D_i is low; if $\mathbf{v}(t) \cdot \mathbf{v}_i(t+1)$ is low, there is too much bending between $\mathbf{v}(t)$ and $\mathbf{v}_i(t+1)$. So fiber tracking should be terminated at channel D_i when anyone of the above quantities is low. This could simply be done by setting a threshold to step size so that channels with step size less than this threshold are terminated. The threshold is a statistical value obtained through a large size of experiments. This self adapting step size constrains propagation speed in regions with high curvature or low diffusion anisotropy while increases speed in regions with low curvature or high diffusion anisotropy, it also automatically terminates fiber tracking at channel(s) with extremely low step size(s).

4. EXPERIMENTAL RESULTS

In this section we present synthetic as well as real data experimental results. We did experiments on a set of subjects, but only list results of one subject for demonstration.

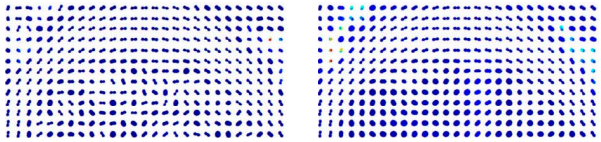

(a) (b)

Fig. 1. (a)-(b)Images of ADC profile $\mathbf{u}^T D_1 \mathbf{u}$ with D_1 the solution of Parker's method and proposed model(4) respectively.

The first experiment is to demonstrate the superiority of the proposed model (4) over Parker et. al's method[6] in recovering smooth multi-tensor field as well as the volume fraction f using human brain HARD MRI data. The data set consists of 33 diffusion weighted images as well as one image in the absence of a diffusion-sensitizing field gradient. 27 evenly spaced axial planes with 128×128 voxels in each slice are obtained using a 3T MRI scanner with a single shot spin-echo EPI sequence. Slice thickness is $3.8mm$, gap is 0 between two consecutive slices , repetition time $(TR) = 1000ms$, $echotime(TE) = 85ms$ and $b = 1000s/mm^2$, and the field of view (FOV) = $200mm \times 200mm$. Fig.1$(a)-(b)$ compare maps of apparent diffusion coefficient(ADC) profiles corresponding to D_1, i.e. $\mathbf{u}^T D_1 \mathbf{u}$ using solutions obtained from Parker et.al's([6]) and proposed model(4) respectively. The region is chosen around corpus callosum in one slice of the human brain. In Fig.1(a) shapes of ADC profile varies a lot from voxel to voxel, especially in regions outside the corpus callosum. In comparison, in Fig.1(b), shapes of ADC profile change smoothly from voxel to voxel, and in the region below corpus callosum, voxels which are most likely to be of isotropic diffusion have sphere-shaped ADC, this is more consistent with the neuroanatomy.

The second experiment is to show MTEND algorithm outdoes TEND algorithm in reconstructing fiber traces with bifurcation involved. This is done on a simulated diffusion tensor field with bifurcation of fiber traces expected to appear on the boundary between portion of the field with one tensor and the other portion with two diffusion tensors. We firstly simulate a $20 \times 20 \times 3$ multi-vector field shown in blue arrows in Fig.2(a)(b). At each voxel, one arrow corresponds to principal eigenvector of a diffusion tensor. So there would be two diffusion tensors at location with two arrows while one tensor at location with only one arrow. Secondly, we construct a multi-tensor field so that the multi-vector field is the corresponding principle eigenvector field. MTEND algorithm is applied to the multi-tensor field and the result is shown in Fig.2(a). Notice TEND is applied on single tensor field, we then construct raw DTI data based on the simulated multi-tensor field using(3) with $s_0 = 400, b = 1000$, $f = 1$ at voxels with one vector,$f = .5$ at voxels with two vectors, and 33 $\mathbf{u}$'s which are uniformly distributed on a sphere. Single tensor field could finally

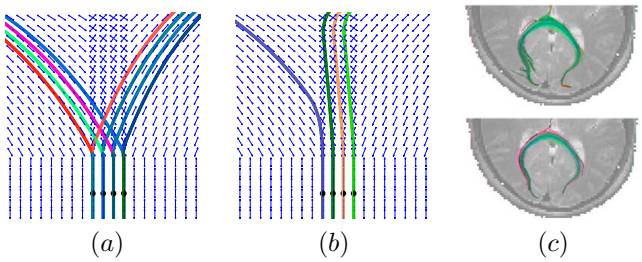

(a) (b) (c)

Fig. 2. (a) Traces recovered by using MTEND based on simulated multi-tensor field, the black points at the bottom are seeds. (b) Traces recovered by using TEND based on the corresponding reconstructed DTI data. (c) Axial view of fiber tracking results in corpus callosum region using MTEND(top),TEND(bottom) algorithm resp.

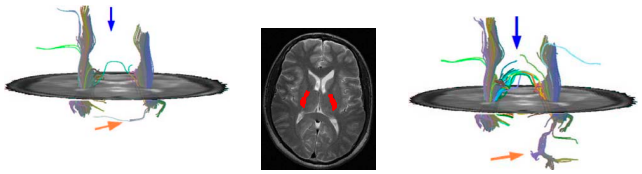

(a) (b) (c)

Fig. 3. (a)(c) are tracking results using TEND, MTEND method respectively. (b) Anatomic image of one slice with red regions the seeds of tracking.

be reconstructed using least-squares method based on DTI model. Applying TEND algorithm to the single-tensor field we obtain result shown in Fig.2(b). In Fig.2(a)(b) the four black points are seeds of the fiber tracking. Nice bifurcations are observed in Fig.2(a), and they take place on the boundary between the single tensor field and the two-tensor field as expected. In comparison, no bifurcation is visualized from Fig.2(b) and only the most left fiber trace goes almost along the vector field, while the other 3 fiber traces do not make sense at all. This verifies the accuracy of MTEND algorithm based on multi-tensor field outdoes TEND based on single-tensor field in recovering fibers with branching.

Next, fiber tracking results on human brain HARD MRI data are shown. The main aim is to show that MTEND and TEND work similarly in the corpus callosum region where Gaussian diffusion is dominant. But they differ in regions with non-Gaussian diffusion. Fig.2(c) shows axial view of tracking results around the corpus callosum region using MTEND(top),TEND(bottom) algorithm. The tracking results are embedded on a 2D anatomic image. Tracking starts from a small portion inside the corpus callosum. No significant difference is observed as in corpus callosum region, Gaussian distribution is dominant, biGuassian model with $f \simeq 1$ and Gaussian model work equivalently in recovering a single-tensor field.

Finally, we select two regions of interest(ROI) from the internal capsule(red region in Fig.3(b)) for another set of

comparison. We set all voxels with high anisotropy in the whole brain volume as seeds, then apply MTEND based on multi-tensor field recovered using model(4) and TEND based on single-tensor field recovered using Guassian diffusion model to reconstruct fiber traces separately. In MTEND we set $\gamma = 0.9$, threshold of step size δ to be 0.1 which is obtained from a large size of experiments. Only those fibers passing through the ROIs are retained and shown in Fig.3(a)(c) for TEND and MTEND respectively. Clearly, MTEND method recovers more branching fibers than TEND method does and these branching fibers are reasonable from the view point of neuroanatomy. Specifically, it happens in 3 different locations: the first one is at the lower right corner and directed by orange arrow. Bunches of fiber traces with several branches are nicely shown up in Fig.3(c), but they do not appear in Fig.3(a). The second one is located at the middle and directed by blue arrow. A strong bundle connecting the left portion and the right portion is clearly visualized in Fig.3(c) but only one fiber trace is shown in Fig.3(a). The third one lies in the most upper left position: Fig.3(c) looks thicker and includes more fibers in each branching than Fig.3(a) does. The main reason for the difference is that voxels involving branching in MTEND method are characterized as isotropic, so TEND algorithm terminates at these voxels.

5. CONCLUSION

A new variational framework for simultaneous reconstruction and regularization of multi-diffusion tensor field together with a new fiber tractography algorithm based on multi-tensor field are provided. The performance of the proposed model has been evaluated on synthetic data and several human brain HARD MR images. The experimental results indicate that proposed model(4) for recovering multi-tensor field together with MTEND for reconstruction of white matter fiber traces work more accurately than Gaussian diffusion model together with TEND.

The proposed model is under the assumption that the probability density function of diffusion is of linear combination of two Gaussians. This results in 13 unknowns at each voxel, and hence at least 13 diffusion weighted images acquisition is required to solved out 13 unknowns accurately. Model that does not require specific assumption on diffusion and that requires less diffusion weighted images will be addressed in separate papers.

6. REFERENCES

[1] D. Le Bihan, E. Brethon, D. Lallemand, P. Grenier, E. Cabanis, and M. Laval-Jeantet, "Mr imaging of intravoxel incoherent motions: Application to diffusion and perfusion in neurologic disorders," *Radiology*, vol. 161, pp. 401–407, 1986.

[2] PJ Basser, J Mattiello, and D LeBihan, "Mr diffusion tensor spectroscopy and imaging," *Biophys*, vol. 66:259, pp. 267, 1994.

[3] A.L.Alexander, K.M.Hasan, M.Lazar, J.S.Tsuruda, and D.L.Parker, "Analysis of partial volume effects in diffusion-tensor mri," *Magn Reson Med*, vol. 45, pp. 770–780, 2001.

[4] LR Frank, "Anisotropy in high angular resolution diffusion-weighted mri," *Magn Reson Med*, vol. 45, pp. 935–939, 2001.

[5] DS Tuch, RM Weisskoff, JW Belliveau, and VJ Wedeen, "High angular resolution diffusion imaging of the human brain," in *Proc. of the 7th ISMRM*, Philadelphia, 1999, p. 321.

[6] G.J.M.Parker and D.C.Alexander, "Probabilistic monte carlo based mapping of cerebral connections utilizing whole-brain crossing fiber information," in *Information Processing in Medical Imaging*, Ambleside UK, 07 2003, pp. 684–696.

[7] D.S.Tuch, T.G. Reese, M.R. Wiegell, N.Makris, J.W. Belliveau, and V.J. Wedeen, "High angular resolution diffusion imaging reveals intravoxel white matter fiber heterogeneity," *Magn Reson Med*, vol. 48, pp. 577–582, 2002.

[8] B. C. Vemuri, Y. Chen, M. Rao, Z. Wang, T. McGraw, T. Mareci, S.J. Blackband, and P. Reier, "Automatic fiber tractograph from dti and its validation," in *Proc. of 1st IEEE International Symposium on Biomedical Imaging*, 2002, pp. 505–508.

[9] C. Pierpaoli, P. Jezzard, P.J. Basser, A. Barnett, and G. Di Chiro, "Diffusion tensor mr imaging of the human brain," *Radiology*, vol. 201(3), pp. 637–648, 1996.

[10] Rachid Deriche, David Tschumperle, and Christophe Lenglet, "Dt-mri estimation, regularization and fiber tractography," in *Proc. of 2nd ISBI*, Washington D.C, 2004, pp. 9–12.

[11] C.-F. Westin, S. E. Maier, B. Khidir, P. Everett, F.A. JoleszH., and R. Kikinis, "Image processing for diffusion tensor magnetic resonance imaging," in *Lecture notes in computer science:MICCAI*, Cambridege:Springer, 1999, pp. 441–452.

[12] M.Lazar, D.M.Weinstein, J.S. Tsuruda, Khader M. Hasan, K. Arfanakis, M. Meyerand, B. Badie, H. Rowley, V. Haughton, A. Field, and A. Alexander, "White matter tractography using diffusion tensor deflection," *Human Brain Mapping*, vol. 18, pp. 306–321, 2003.